Research on Chemical Intermediates (2019) 45:2529–2547
https://doi.org/10.1007/s11164-019-03750-2

Sunlight-induced photocatalytic degradation of acetaminophen over efficient carbon doped TiO_2 ($CTiO_2$) nanoparticles

Yasser A. Shaban[1,2] · **Hasna M. Fallata**[1]

Received: 25 September 2018 / Accepted: 18 January 2019 / Published online: 28 January 2019

Abstract

Carbon doped titanium oxide ($CTiO_2$) photocatalyst was successfully synthesized by the sol–gel method. The crystal structure, surface morphology, and optical properties of $CTiO_2$ have been characterized by X-ray diffraction, Brunauer–Emmett–Teller surface area (S_{BET}), scanning electron microscope, UV–Vis, X-ray spectroscopy (EDS), Fourier transform infrared and X-ray photoelectron spectroscopy. The photocatalytic degradation of acetaminophen (AMP) in aqueous solution, seawater, and polluted seawater has been investigated by using the synthesized photocatalyst under irradiation of UV and natural sunlight. The effectiveness of $CTiO_2$ compared to pure TiO_2 toward the photocatalytic removal of AMP was significantly observed. The optimized conditions including catalyst dose, initial concentration of AMP and solution pH were also studied for effective photocatalytic removal. The highest degradation rate was obtained when 2.0 g L^{-1} of the catalyst was used at pH 7. The kinetic results revealed that the photocatalytic degradation of AMP using $CTiO_2$ obeyed a pseudo-first-order reaction kinetics.

Keywords Acetaminophen · Photocatalytic degradation · $CTiO_2$ · Nanoparticles · Seawater · Sunlight

Electronic supplementary material The online version of this article (https://doi.org/10.1007/s11164-019-03750-2) contains supplementary material, which is available to authorized users.

✉ Yasser A. Shaban
ydomah@kau.edu.sa; yasrsh@yahoo.com

[1] Marine Chemistry Department, Faculty of Marine Sciences, King Abdulaziz University, P.O. Box 80207, Jeddah 21589, Saudi Arabia

[2] National Institute of Oceanography and Fisheries, Qayet Bay, Alexandria, Egypt

Introduction

The introduction of pharmaceutical compounds into aquatic environments has become a major concern, as they can constitute a potential risk for the ecosystem even at low concentrations. These compounds can reach the aquatic ecosystem by various ways, such as veterinary and human excretion residues, direct discharge of surplus drugs, and ineffective treatment of the pharmaceutical industrial effluents [1–4]. As a consequence of their continuous input, persistence nature, in addition to the inadequacy of the conventional treatment techniques, they have been widely detected in different environmental matrices. A large variety of pharmaceuticals have been determined at levels ranging from ppb to ppm in sewage effluents of treatment plants, natural waters, rivers and even in drinking water [5, 6]. Among these pharmaceuticals, acetaminophen (AMP) is one of the leading drugs in terms of the use as a common analgesic and antipyretic. As a result of its widespread application and massive use, it has been detected in considerable levels in treated wastewater [7], in natural water [8] and in rivers [9].

Limitations associated with conventional technologies employed in the wastewater treatment plants such as partial degradation of pharmaceuticals and production of secondary contaminants have been reported by several studies [10–12]. Hence, innovation of an effective and economically viable method for degradation of these persistent compounds in order to minimize their amounts discharged into the environment is a challenging topic.

In this context, TiO_2 photocatalysis has been proved to be one of the most promising remedy technologies for the removal of environmental pollutants, due to the key advantages of the photocatalyst such as economic viability, photo-stability and non-toxicity [13–22]. However, TiO_2 can only be excited by UV light (i.e. $\lambda < 380$ nm), which significantly confines its wide and viable application. Recent studies have shown that carbon modification of TiO_2 can effectively broaden its utilizable range of light to the visible region [14, 20–24].

Most of the previous photocatalysis studies that focus on the destruction of pharmaceuticals were carried out in simulated wastewater and under artificial UV light. However, utilization of TiO_2 nanoparticles has not been reported for the elimination of AMP from real polluted wastewater/seawater under natural sunlight illumination. In this study, carbon doped titanium oxide ($CTiO_2$) nanoparticles will be synthesized, characterized, and employed to eliminate AMP, as a model of pharmaceuticals, from aqueous, seawater, and real polluted seawater samples under UV and natural sunlight illumination. To the best of our knowledge, this is the first time for employing $CTiO_2$ for the remediation of AMP in natural seawater under real solar light. Catalyst dosage, initial concentration of AMP, and solution pH will be investigated and optimized.

Experimental

Preparation of the catalysts

Titanium (IV) butoxide (TBT) was used as a precursor of both Ti and C, while glycine (NH_2CH_2COOH) was used as an additional source of C. First, 10 mL of TBT was slowly added into an equal volume of absolute ethanol. Then, 5 mL of 0.1 M of glycine solution (prepared in ultrapure Milli-Q water) was added dropwise to a titanium solution under ultrasonication. The pH was adjusted between 3 and 3.5 using nitric acid (HNO_3) to control nanocrystalline shape. In order to form sols, the solution was vigorously stirred for 2 h then the formed sols were transformed into gels by aging for 24 h. Finally, the desired $CTiO_2$ nanoparticles were formed by drying the gel at 100 °C for 12 h, followed by calcination at 500 °C for 2 h. For comparison, pure TiO_2 (LOBA, India) was used as a standard reference catalyst without any further modification.

Catalyst characterization

The crystal structure of the photocatalysts was examined through a X-ray diffractometer (Shimadzu, XRD-6000) with crystal monochromated CuK_α radiation with an accelerating voltage of 40 kV and a current of 30 mA. XRD patterns were recorded in the angular range of $2\theta = 20°–70°$ at a scan rate of 1.0° min^{-1}. The optical properties of the photocatalysts were evaluated by a Shimadzu, PharmaSpec UV-1700 Spectrophotometer. A Brunauer–Emmett–Teller (Quantachrome instrument) was employed for the determination of the surface area (S_{BET}) of the photocatalysts. The surface morphology of the photocatalysts was studied using a JSM-7600F, JEOL (USA) Scanning Electron Microscope (SEM). The elemental composition was analyzed by means of energy dispersive X-ray spectroscopy (EDS, X-Max 50 mm^2, Oxford Instruments). To obtain further information on the chemical structure and functional groups present in the photocatalysts, Fourier Transform Infrared (FT-IR) spectra were recorded on a Perkin Elmer FT-IR spectrometer, scans were recorded over the wave range of 400–4000 cm^{-1}. X-ray photoelectron spectroscopy (XPS, SPECS surface analysis systems) was used to characterize the elemental composition of the catalyst surface and its chemical state. The XPS measurements were carried out at a base pressure of 4×10^{-10} mbar. A dual anode non-monochromatic Mg–K_α (1253.6 eV) X-ray source was used at an operating power of 13.5 kV and 150 W 15 kV.

Photocatalytic removal experiments

Polluted and clean seawater samples were collected from Al-Arbaeen Lagoon and Sharm Obhur (Jeddah, KSA), respectively. Ionic composition and chemical characteristics of the studied clean and polluted seawater samples are listed in Table S1 (supplementary Material). Samples were filtered through Whatman GF/C in order

to remove any solid particles. Both clean seawater samples and aqueous solutions (deionized water) were spiked with different loads of acetaminophen (GlaxoSmith-Kline) ranging from 2.0 to 10 ppm. A Pyrex glass reactor (500-mL) containing both the samples to be treated and the photocatalyst under continuous magnetic stirring was used as a reaction vessel to carry out all photocalaytic experiments. To ensure the establishment of an adsorption/desorption equilibrium, the suspension was magnetically stirred in the dark condition for 30 min. Then, the photoreactor was placed inside a fluorescence chamber (CC-80, Spectroline) equipped with a 15 W low pressure UV lamp (Upland, 365 nm, 65 W m^{-2}). All solar photocatalytic experiments were carried out by the direct exposure of the photoreactor to natural sunlight during the daytime between 11:00 a.m. to 14:30 p.m. The average solar intensity, recorded by Field Scout Light Sensor Reader (Spectrum Technologies, Inc.) equipped with 3670i Silicon Pyranometer Sensor, was found to be 1140 $Wm^{-2.}$

At regular intervals, several milliliters of the treated samples were withdrawn from the reactor and centrifuged to eliminate the photocatalyst. The AMP content was immediately analyzed by using a UV–visible spectrophotometer (UV-1700 PharnaSpec, Shimadzu) at $\lambda = 243$ nm.

Results and discussion

Catalyst characterization

X-ray diffraction, particle size and surface area analysis

The XRD analysis was carried out to study the crystallinity and to calculate the crystallite size of the prepared photocatalysts. As shown in Fig. 1, the major diffraction peaks are indexed as (101), (004), (200), (105), (211), (204) and (116), indicating a typical pattern of anatase for both catalysts. The absence of a carbon peak

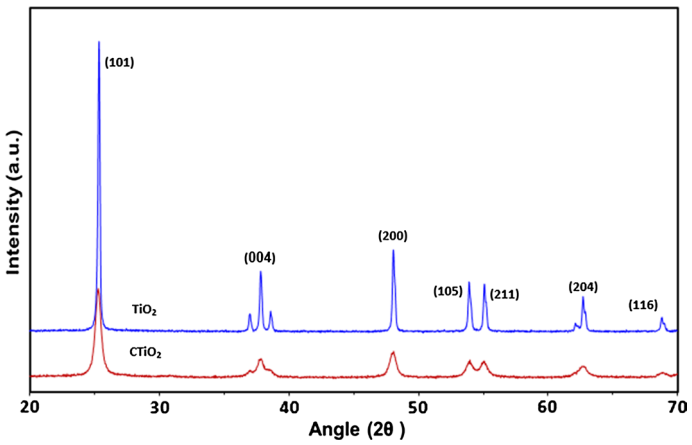

Fig. 1 XRD patterns of the photocatalysts

revealed that the structure of $CTiO_2$ is not altered by carbon incorporation. Using Debye–Scherrer's equation, the crystallite sizes of TiO_2 and $CTiO_2$ nanoparticles were calculated:

$$D = k\lambda/(\beta \cos\theta), \tag{1}$$

where D is the average crystallite size (nm), k is the Scherer's constant of the order of unity, λ is the X-ray wavelength, θ is the diffraction angle, and β is a full width at half the maximum (FWHM) of the diffraction line observed. The average crystallite sizes of TiO_2 and $CTiO_2$ were calculated to be about 44.3 nm and 15.7 nm, respectively. The observed broadening of XRD peaks of $CTiO_2$ and the decline of their intensities compared to those of pure TiO_2 are in accordance with the smaller crystal sizes of $CTiO_2$ [25–27]. The specific surface areas for $CTiO_2$ and TiO_2 determined by BET were found to be 101 and 44 $m^2\ g^{-1}$, respectively. It has been reported by several authors that the doping of TiO_2 via the sol–gel method can increase its specific surface area due to the disturbance of the hydrolysis-condensation reactions of the titanium alkoxide precursor [28, 29]. Manoharan and Sankaran [30] suggested that the increase of the specific surface area of non-metal-doped TiO_2 may be due to the replacement of Ti or/and O in the TiO_2 lattice by the dopant atom. The increase of the surface area upon the modification by carbon for $CTiO_2$ may result in an enhancement of its photocatalytic performance.

Surface morphology

The surface morphology of TiO_2 and $CTiO_2$ was examined using SEM. As can be seen from the SEM micrographs of the photocatalysts (Figure S1, supplementary Material), $CTiO_2$ shows smaller crystals (Fig. S1b) compared to those of TiO_2 (Fig. S1a), which agrees with the aforementioned XRD-based crystal sizes calculations. Figure 2 displays the EDS spectra of both catalysts. Only Ti and O peaks are shown for pure TiO_2, whereas carbon peak is clearly defined for $CTiO_2$ with atomic% of 5.6%, evidencing the successful incorporation of carbon into $CTiO_2$.

Optical properties

The UV–Vis absorption and the optical bandgap energy of $CTiO_2$ were compared to that of pure TiO_2 (Fig. 3). It is clearly noted that the response of pure TiO_2 is limited only to UV light. The onset of its absorption spectrum was found to be ~ 415 nm. Whereas, the absorption spectrum of $CTiO_2$ is red-shifted to the edge of around 695 nm, revealing a reduction in the bandgap energy value for $CTiO_2$ due to the presence of carbon. The Kubelka–Munk function was used to estimate the optical bandgap energy by plotting the $(\alpha h\upsilon)^{1/2}$, versus photon energy [31, 32]:

$$\alpha h\upsilon = A\left(h\upsilon - E_g\right)^{1/2}, \tag{2}$$

$$(F(R)\, h\upsilon)^n = A\left(h\nu - E_g\right), \tag{3}$$

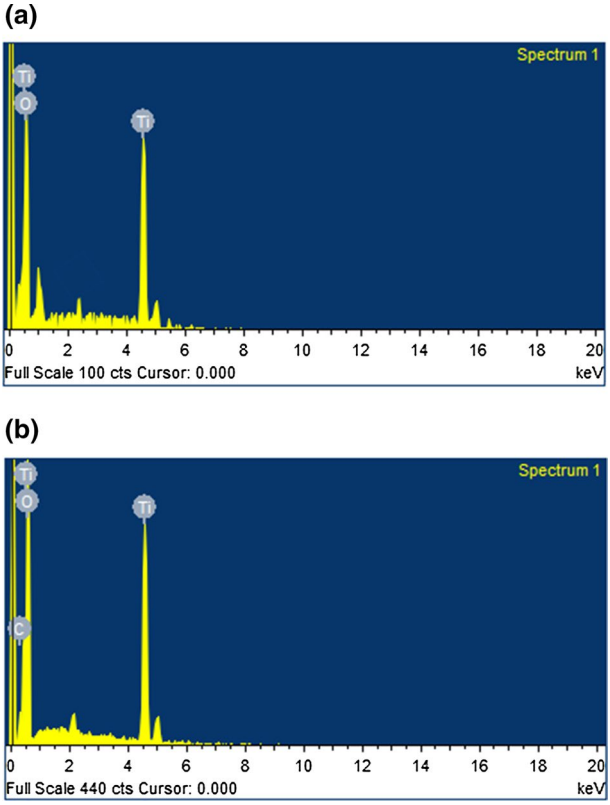

Fig. 2 EDS analysis for TiO_2 (**a**) and $CTiO_2$ (**b**)

where

$$F(R) = (1 - R)^2/2R = \alpha/S, \tag{4}$$

where α, h, υ, E_g, A, R and S, light absorption coefficient of the semiconductor at a certain value of wavelength λ, Planck's constant, frequency of light, optical bandgap energy, optical constant, diffused reflectance, scattering coefficient, respectively). Remarkable narrowing of the bandgap energy to 1.78 eV for $CTiO_2$ is clearly observed (Fig. 4b), which can be attributed to the mixing of the $2p$ orbital of C, acting as an acceptor state, with the $2p$ orbital of O, due to the lower valence electron number of C than that of O [33, 34].

FTIR analysis

To ascertain the surface properties of $CTiO_2$ and TiO_2, FTIR analysis was carried out (Fig. 4). The FT-IR spectrum exhibits peaks at low frequencies (600–900 cm^{-1}), which can be assigned to Ti–O–Ti bridge stretching modes and the Ti–O bond [35, 36]. The broad band at 3000–3500 cm^{-1} corresponds to the surface O–H stretching, whereas the OH bending of adsorbed H_2O molecules on the surfaces of catalyst is

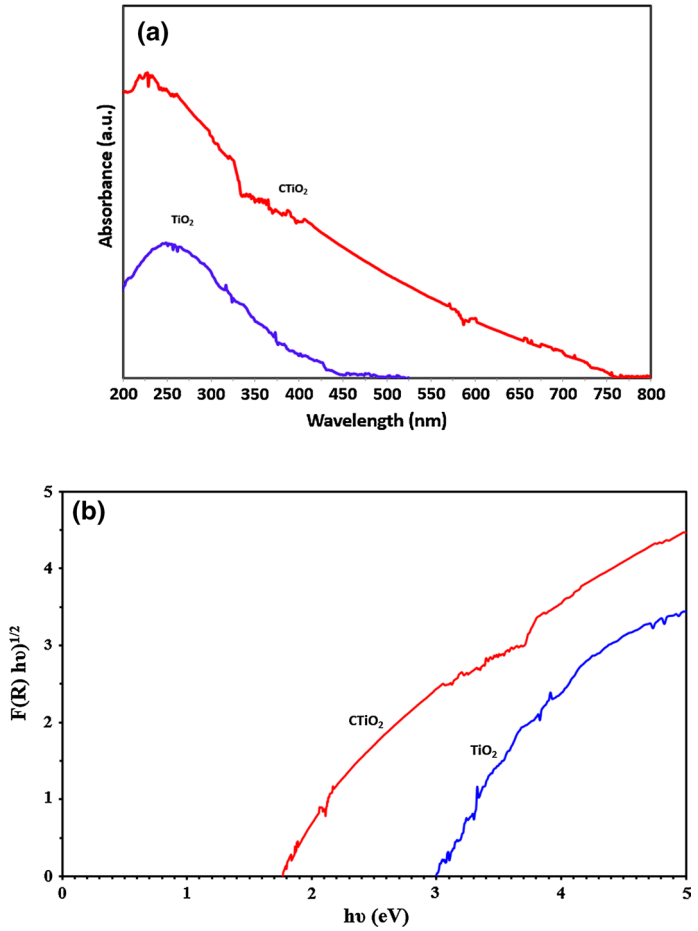

Fig. 3 UV–Vis spectra of TiO_2 and $CTiO_2$ nanoparticles (**a**); the corresponding plot of the transformed Kubelka–Munk function (**b**)

shown by the peak at 1680 cm^{-1} [37–39]. It is worth mentioning that the superficial OH groups of the photocatalyst can significantly improve its photocatalytic activity by suppression of the recombination of the electron–hole pairs as a consequence of the interaction with holes [40–42]. The successful incorporation of carbon into the structural lattice of $CTiO_2$ is clearly verified by the presence of a new carbon band at 2900 cm^{-1} due to C–H stretching.

XPS analysis

To confirm the incorporation of carbon atoms into the TiO_2 lattice, X-ray photoelectron spectroscopy (XPS) was performed (Fig. 5). The XPS survey spectrum (Fig. 5a) revealed the presence of Ti, O, and C in $CTiO_2$. The Ti 2*p* spectrum in

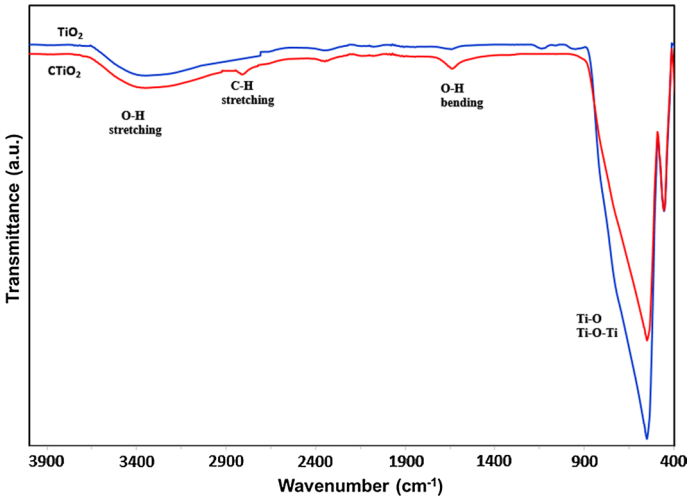

Fig. 4 FTIR for TiO_2 and $CTiO_2$ nanoparticles

Fig. 5b demonstrates the two spin–orbit components of Ti2p–2$p_{3/2}$ at 458.4 eV and Ti–2$p_{1/2}$ at 464.3 eV. The approximately 5.8 eV difference between their energies indicates the existence of Ti in the oxidation state of Ti^{4+} [43, 44]. Figure 5c shows the O 1s XPS spectrum indicates the presence of three peaks. The first peak at 529.8 eV represents the lattice oxygen bound to Ti (Ti–O, Ti–O–Ti). The two other peaks at 531.5 and 533.8 eV are resulting mainly from the influence of the chemisorbed H_2O or the free OH on the sample surface [45, 46]. The C 1s XPS spectrum include a strong peak at 285.0 eV, suggesting the existence of C as C–C (Fig. 5d). The other two small peaks are centered at 286.7 and 288.8 eV, revealing the presence of C–O/C=O and O–C=O, respectively [46, 47]. The XPS results indicate that the carbon doped TiO_2 has an atomic composition of 38.4% Ti2p, 42.2% O 1s and 19.4% C 1s, revealing the successful incorporation of carbon atoms into the TiO_2 lattice. The observed discrepancy between the atomic% of carbon obtained by EDS (5.6%) and XPS (19.4%) can be attributed to the different types of the incident energies of the two probes, electron (for EDS) and X-ray (for XPS). The XPS results represent the quantitative analysis at the catalyst surface, whereas those of EDS denote the content at deeper layers (i.e., near-bulk property) [48]. Accordingly, the obtained results evidenced the incorporation of carbon at different depths of $CTiO_2$ surface.

Effect of catalyst loading

The effect of catalyst dose of $CTiO_2$ on the photodegradation of AMP (3.0 ppm) under illumination of UV light is shown in Fig. 6. The photodegradation rate of AMP increased when the concentration of $CTiO_2$ was elevated from 0.5 to 2.0 g L^{-1}. Further increment in catalyst loading led to a remarkable decrease in the photodegradation rate, revealing an optimal catalyst loading of 2.0 g L^{-1}. In general, the rate of photocatalytic degradation increases with the increase of photocatalyst

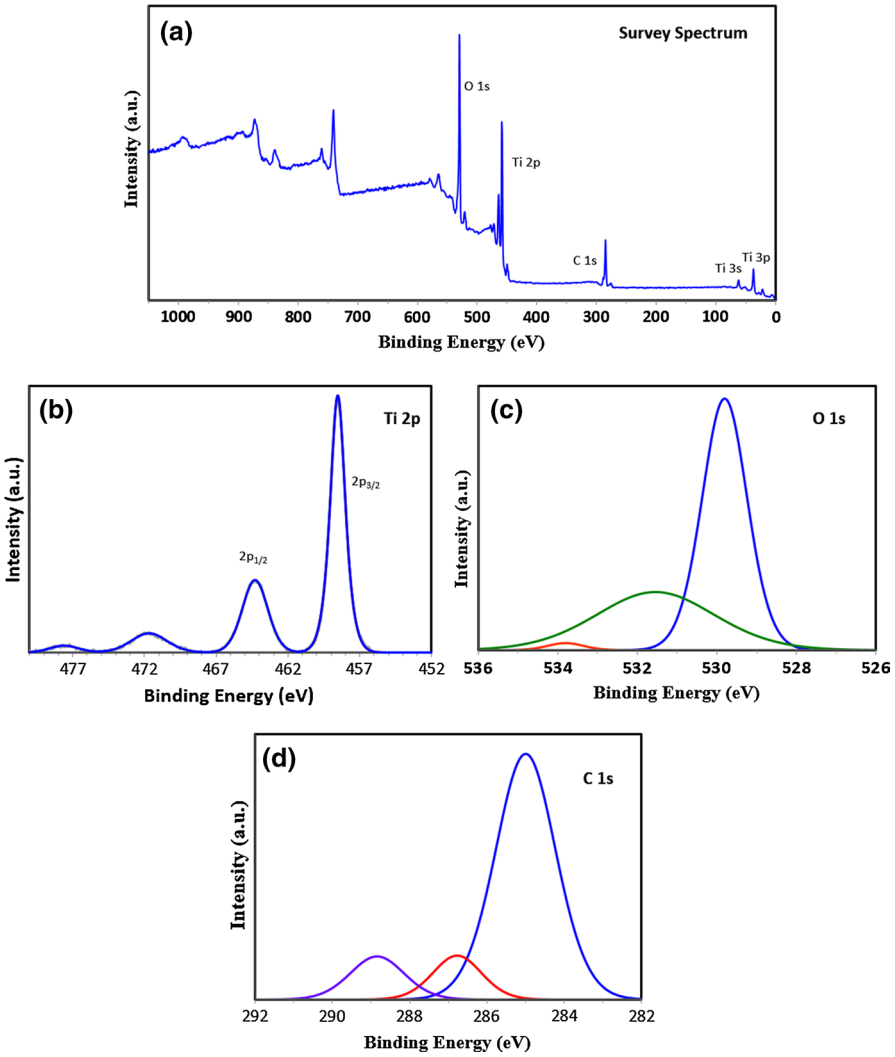

Fig. 5 X-ray photoelectron spectroscopy (XPS) for $CTiO_2$

dosage due to the increase in active sites [49–51]. This is mainly due to the increase of hydroxyl radicals produced from irradiated photocatalysts [52, 53]. At lower catalyst loading, less transmitted radiation can be utilized in the photocatalytic reaction, consequently, a decline in the degradation rate will be observed [54, 55]. However, beyond the optimum amount of catalyst loading, the degradation rate might be reduced due to the decrease of the degree of transparency of the suspension, and thus increasing the light scattering and also the penetration depth of the photons is diminished and less photocatalysts could be activated [56, 57]. Additionally, agglomeration of nanoparticles at high concentrations results in a decline in both

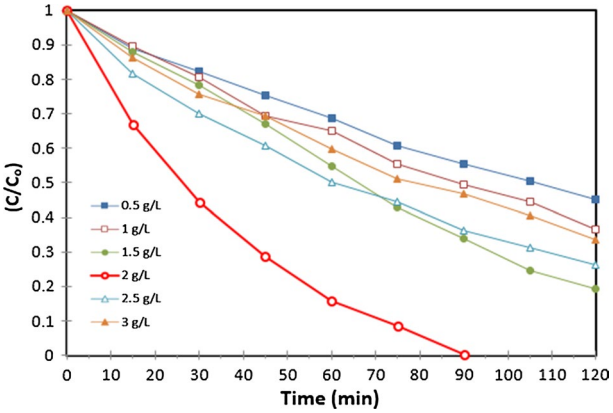

Fig. 6 Effect of catalyst dose on the photocatalytic degradation of acetaminophen (3.0 ppm) under illumination of UV light

the surface area and the number of active sites available for light absorption and photocatalytic degradation [52, 53, 58, 59] and, hence, a drop in the photocatalytic degradation efficiency of the catalyst.

Effect of pH

Solution pH plays a vital role in the photocatalytic activity of the photocatalyst, as it influences the surface charge and the oxidation potential of photocatalyst and the adsorption and the dissociation of the organic molecule on the catalyst surface [60, 61]. Figure 7 shows the photodegradation of AMP in the presence of the optimum

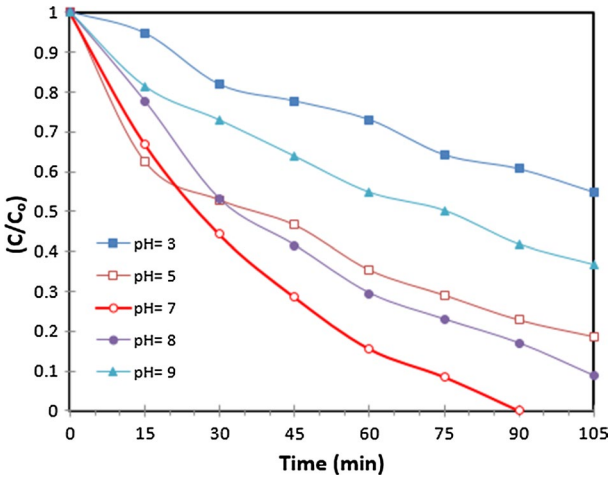

Fig. 7 Effect of pH on the photocatalytic degradation of acetaminophen using 2.0 g L^{-1} of $CTiO_2$ under illumination of UV light

loading of $CTiO_2$ (2.0 g L^{-1}) at various pH values ranging between 3 and 9. As can be seen, the photodegradation efficiency of AMP enhanced with increasing the solution pH up to 7, followed by a significant decline with the subsequent elevation of pH, indicating an optimum pH value of 7. In neutral medium, the adsorption of AMP onto the catalyst surface is maximum, due to the presence of AMP in its nonionic form, and the water solubility is minimum. On the other hand, the significant decline in the degradation rate at high pH value of 9.0, can be attributed to the surface ionization of the photocatalyst. The TiO_2 surface is negatively charged in alkaline media, where solution pH is higher than pH at point of zero charge ($pH_{PZC} = 6.3$) [3].

$$TiOH + OH^- \rightarrow TiO^- + H_2O \tag{5}$$

Furthermore, at higher pH, the reduction of oxygen by electrons to form superoxide radical anion ($O_2^{-\cdot}$) can be suppressed (Eq. 6), resulting in less formation of H_2O_2 and $^{\cdot}OH$ (Eqs. 7–9), and subsequently lower degradation rate of AMP.

$$O_2^{-\cdot} + H^+ \rightarrow HO_2^{\cdot} \tag{6}$$

$$HO_2^{\cdot} + H^+ + e_{cb}^- \rightarrow H_2O_2 \tag{7}$$

$$e_{cb}^- + H_2O_2 \rightarrow {}^{\cdot}OH + {}^-OH \tag{8}$$

$$H_2O_2 + h\nu \rightarrow 2\,{}^{\cdot}OH \tag{9}$$

$$TiOH + H^+ \leftrightarrow TiOH^{2+} \tag{10}$$

Whereas, in acidic medium where solution pH is lower than pH_{PZC} of TiO_2, its surface is dominated by the positive charge. In the meantime, AMP is primarily in its nonionic form, which decreases the electrostatic attraction between TiO_2 surface and AMP [3] which consequently, lowers the degradation rate of acetaminophen.

Effect of initial AMP concentration

The effect of initial concentration of organic pollutants on their photocatalytic degradation is one of the main factors that needs to be taken under consideration. Generally, higher initial concentration of organic compound reduces the photocatalytic degradation efficiency. It might be due to the greater amount of molecules competing to be adsorbed on the surface of the photocatalyst, resulting in a limitation of catalyst active sites required for generating the hydroxyl radicals, which in turn reduces the photocatalytic activity of the catalyst [56]. In addition, at very high concentrations of organic compound, the generation of electron–hole pairs is greatly reduced, due to much of the light is screened as less number of photons are able to reach the surface of photocatalysts [62, 63]. The extension of the irradiation time required for complete removal of AMP at the best experimental conditions of pH 7 and 2.0 g L^{-1} of $CTiO_2$ under UV light with the increment in its initial concentration is clearly noted (Fig. 8). When the initial concentration of AMP is relatively low, the catalyst action inhibition does not occur. Nevertheless, when the AMP initial concentration

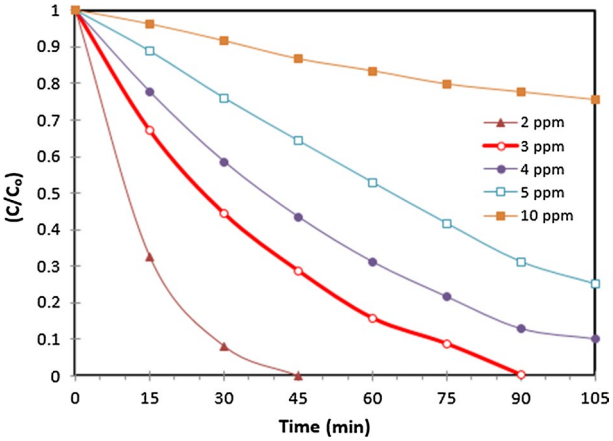

Fig. 8 Effect of initial concentration of acetaminophen on its photocatalytic degradation at the optimal conditions of pH 3 and 2.0 g L^{-1} C-TiO_2 under illumination of UV light

increases, more AMP particles are adsorbed on the surface of $CTiO_2$ leading to a reduction of the light intensity reaching to the surface of the photocatalyst, in addition to the generation of more intermediates compounds which may adsorb onto the catalyst surface. Thus, the suppression of electron–hole pairs is greatly enhanced, leading to a decline in the degradation rate of AMP [64].

Photodegradation kinetics

The kinetics of the photocatalytic degradation of AMP was investigated using the apparent first order reaction equation [65–67]:

$$\mathrm{Ln}\left(C_o / C\right) = k_{app} t, \tag{11}$$

where C_o is the initial concentration of AMP, C is its concentration at irradiation time t. Plotting of $\mathrm{Ln}(C_o/C)$ versus t plot gives a straight line, and its slope is the apparent rate constant k_{app}. Figure 9 shows the kinetic analysis for the photocatalytic degradation of various AMP concentrations (2–10 ppm) at the optimal conditions of pH 7.0 and 2.0 g L^{-1} of $CTiO_2$ under illumination of UV light. The obtained straight lines revealed that the photocatalytic degradation of AMP by using $CTiO_2$ can be described by pseudo-first order kinetics.

Photocatalytic removal of AMP from aqueous solution

The photocatalytic degradation of AMP was evaluated in the presence of the photocatalysts ($CTiO_2$ and TiO_2) under dark and light conditions. Furthermore, the removal of AMP was tested without the photocatalyst (i.e., only light) as a blank experiment (Fig. 10). As can be seen, under photolysis conditions, when no catalyst was added, the removal efficiency of AMP in the presence of UV (Fig. 10a) and

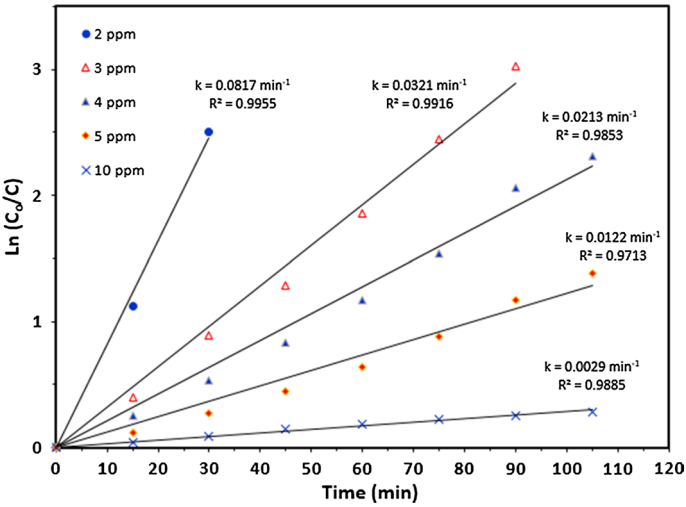

Fig. 9 Kinetic analysis for the photocatalytic degradation of various concentrations of acetaminophen (2–10 ppm) at the optimal conditions of pH 7.0 and 2.0 g L^{-1} of $CTiO_2$ under illumination of UV light

sunlight (Fig. 10b) is less than 5%. On the other hand, there is insignificant removal of AMP through the adsorption process by both catalysts after 90 min in darkness conditions. It is clearly noted that, complete degradation of AMP (3.0 ppm) using 2.0 g L^{-1} of $CTiO_2$ was achieved after only 90 and 75 min of illumination by UV (Fig. 10a) and sunlight (Fig. 10b), respectively. Whereas, the removal efficiency significantly declined when pure TiO_2 was employed. The higher activity of $CTiO_2$ under UV than the pure TiO_2 can be attributed to the smaller particle size of $CTiO_2$ (15.7 nm) than that of pure TiO_2 (44.3 nm). Furthermore, the increase of the surface area of $CTiO_2$ (101 m^2 g^{-1}) compared to TiO_2 (44 m^2 g^{-1}) may result in an enhancement of its photocatalytic performance. Besides these two factors, the significant higher degradation ability of $CTiO_2$ under sunlight could be simply accounted for lowering its bandgap energy as a result of carbon incorporation.

Photocatalytic removal of AMP from seawater

It is imperative to study the effectiveness of the synthesized photocatalyst for the detoxification of different polluted waters having different characteristics. Therefore, the photocatalytic degradation of AMP using $CTiO_2$ was investigated in seawater under dark and light conditions (Fig. 11). Similar to aqueous solution, no obvious elimination of AMP was observed in the absence of light (i.e., only adsorption). Whereas, the degradation efficiency has not exceeded 5% under the photolysis (i.e., only light, without catalyst) conditions. The effectiveness of $CTiO_2$ compared to TiO_2 toward the photocatalytic removal of AMP from seawater under UV (Fig. 11a) and sunlight (Fig. 11b) is certainly significant.

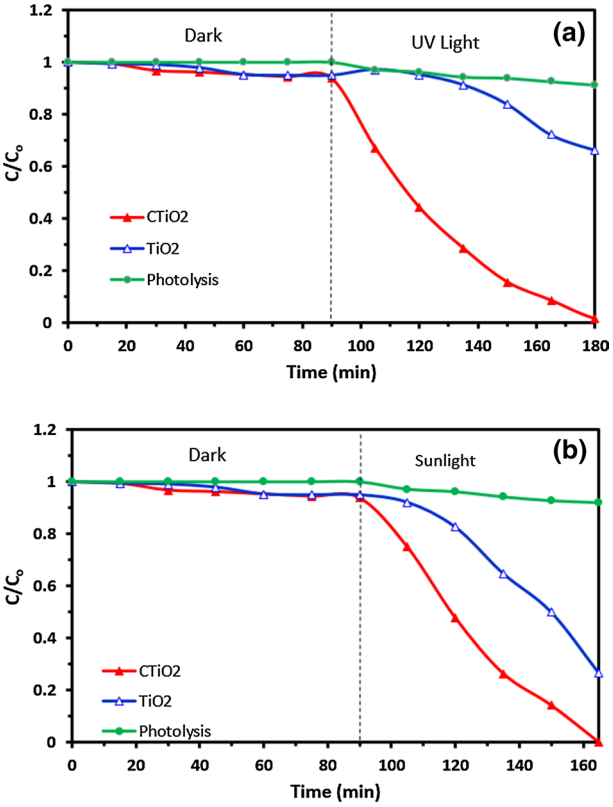

Fig. 10 Removal of acetaminophen from aqueous solution using $CTiO_2$ and TiO_2 photocatalysts under dark and **a** UV light; **b** sunlight illuminations

Photocatalytic removal of AMP from real polluted seawater

It is of great interest to test the applicability of $CTiO_2$ nanoparticles for the detoxification of polluted real seawater samples under natural sunlight. The photocatalytic removal of AMP (0.094 ppm) found in real polluted seawater samples was tested under illumination of sunlight using the optimum catalyst loading of 2.0 g L^{-1}. It is clearly noted from Fig. 12 that $CTiO_2$ is capable of completely degrading AMP after 180 min, despite the presence of many different types of other pollutants that may simultaneously undergo the photocatalytic oxidation/reduction process at the catalyst's surface.

Stability and reusability of the catalyst

The catalyst stability and reusability play an important role in determining the economic viability and practical applicability of the catalyst in large-scale. The stability

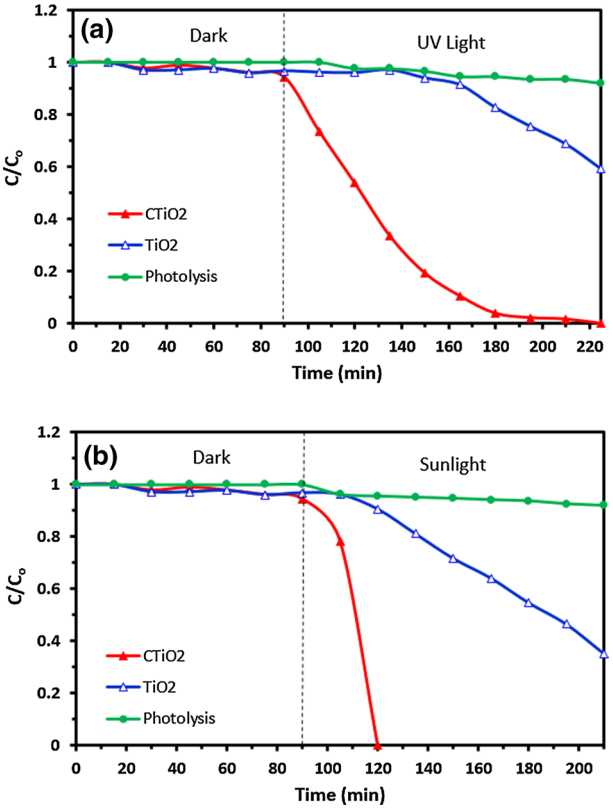

Fig. 11 Removal of acetaminophen from seawater using $CTiO_2$ and TiO_2 photocatalysts under dark and **a** UV light; **b** sunlight illuminations

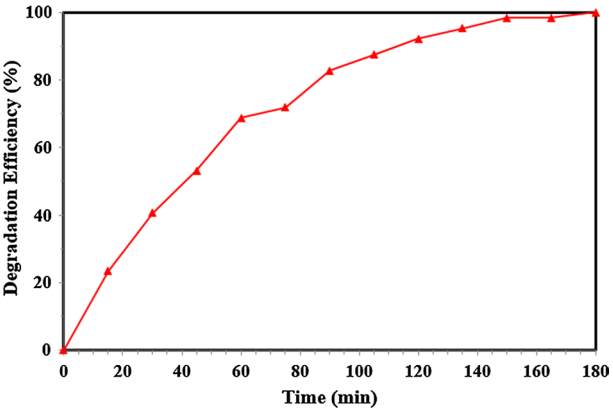

Fig. 12 Removal of acetaminophen from real polluted seawater using $CTiO_2$ photocatalysts under natural sunlight illumination

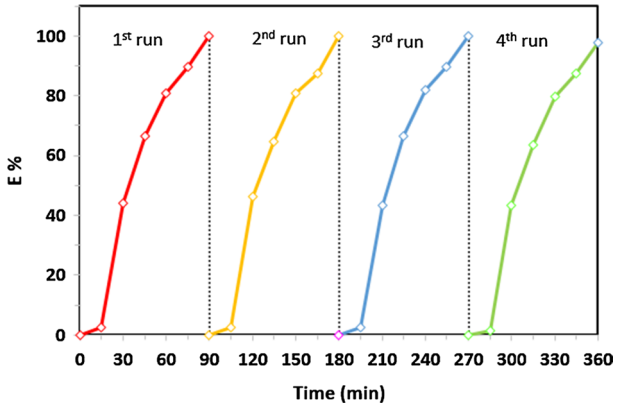

Fig. 13 Cyclic photocatalytic degradation of acetaminophen under illumination of UV light at the optimal conditions

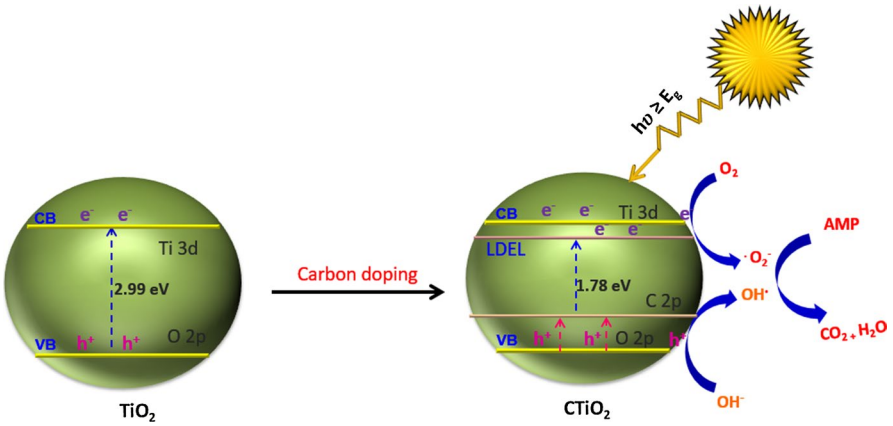

Fig. 14 Simplified photocatalytic degradation mechanism of acetaminophen using $CTiO_2$

of $CTiO_2$ and its ability to reproduce the same measurements were tested over four consecutive repetitions for the degradation of AMP (3.0 ppm) under the same best conditions as shown in Fig. 13. The stability and the potentiality of $CTiO_2$ photocatalyst for continuous reuse is clearly noted by its consistent photoactivity and the similarity of the results obtained after four attempts of the catalyst usage.

Photocatalytic mechanism

As a result of carbon doping, the hybridization of the O 2*p* orbital with C 2*p* orbital leads to a bandgap narrowing for $CTiO_2$. Further reduction of the bandgap can be attributed to the introduction of the localized donor energy level (LDEL) under the conduction band due to the defects and disorders in amorphous TiO_2 (Fig. 14).

Therefore, upon illumination of $CTiO_2$ with light photons of energy ≥ 1.79 eV (the bandgap energy of $CTiO_2$), electron/hole (e^-/h^+) pairs are generated. The electrons in the C 2*p* valence band (e^-) elevate either directly to the conduction band or to the localized donor energy level and then to the conduction band. At the external $CTiO_2$ surface, the positive holes (h^+) oxidize H_2O molecules and/or OH^- ions, whereas the excited electrons (e^-) reduce O_2 to yield reactive oxygen species ($^{\cdot}OH$ and $^{\cdot}O_2^-$), which can be involved in the photocatalytic degradation of AMP.

Conclusion

The photocatalytic degradation of AMP was successfully achieved in aqueous solution, seawater, and real polluted seawater using $CTiO_2$ nanoparticles under both UV and natural sunlight. The highest degradation efficiency was obtained at the favorable conditions of pH 7 and catalyst dose of 2.0 g L^{-1}. The effectiveness of $CTiO_2$ compared to TiO_2 toward the photocatalytic removal of AMP from aqueous solution, seawater, and real polluted seawater under UV and natural sunlight using the $CTiO_2$ nanoparticles is certainly significant. This enhancement could be simply accounted for by lowering its bandgap energy as the result of carbon incorporation for $CTiO_2$.

Acknowledgements The authors would like to thank Mr. Mosa Alzobidi and Dr. Yasar N. K. for their appreciable help in the experimental analysis.

References

1. T. Schwartz, W. Kohnen, B. Jansen, U. Obst, FEMS Microbiol. Ecol. **43**, 325 (2003)
2. F. Baquero, J.L. Martínez, R. Cantón, Curr. Opin. Biotechnol. **19**, 260 (2008)
3. L. Yang, L.E. Yua, M.B. Ray, Water Res. **42**, 3480 (2008)
4. S.C. Antunes, R. Freitas, E. Figuerira, F. Goncalves, B. Nunes, Eniviron. Sci. Pollut. Res. **20**, 6658 (2013)
5. T.H. Heberer, K. Reddersen, A. Mechlinski, Water Sci. Technol. **46**, 1 (2002)
6. A. Nikolaou, S. Meric, D. Fatta, Anal. Bioanal. Chem. **387**, 1225 (2007)
7. T. Ternes, Water Res. **32**, 324 (1998)
8. D.W. Kolpin, E.T. Furlong, M.T. Meyer, E.M. Thurman, S.D. Zaugg, L.B. Barber, H.T. Buxton, Environ. Sci. Technol. **36**, 1202 (2002)
9. P.H. Roberts, K.V. Thomas, Sci. Total Environ. **356**, 143 (2006)
10. M. Carballa, F. Omil, J.M. Lema, M. Llompart, C. Garcia, I. Rodriguez, M. Gomez, T. Ternes, Water Sci. Technol. **52**(8), 29 (2005)
11. M. Petrovic, M.D. Hernando, M.S. Díaz-Cruz, D. Barceló, J. Chromatogr. **1067**(1–2), 1 (2005)
12. J. Radjenovic, M. Petrovic, D. Barcelo, Anal. Bioanal. Chem. **387**(4), 1365 (2007)
13. K. Govindan, S. Murugesan, P. Maruthamuthu, Mater. Res. Bull. **48**, 1913 (2013)
14. Y.A. Shaban, M.A. El Sayed, A.A. El Maradny, R.K. Al Farawati, M.I. Al Zobidi, Chemosphere **91**, 307 (2013)
15. N.H. Nguyen, H. Bai, J. Environ. Sci. **26**, 1180 (2014)
16. L. Szatmáry, J. Subrt, V. Kalousek, J. Mosinger, K. Lang, Catal. Today **230**, 74 (2014)
17. B. Cojocaru, V. Andrei, M. Tudorache, F. Lin, C. Cadigan, R. Richards, V.I. Parvulescu, Catal. Today **284**, 153 (2017)
18. K.A. Gebru, C. Das, J. Water Process Eng. **16**, 1 (2017)
19. P. Shao, J. Tian, W. Shi, S. Gao, F. Cui, J. Mater. Chem. A **3**, 19913 (2015)
20. P. Shao, J. Tian, Z. Zhao, W. Shi, S. Gao, F. Cui, Appl. Surf. Sci. **324**, 35 (2015)

21. Y.N. Kavil, Y.A. Shaban, R.K. Al Farawati, M.I. Orif, M. Zobidi, S.U.M. Khan, Photochem. Photobiol. A: Chem. **327**, 244 (2017)
22. Y. Yang, Y. Li, J. Wang, J. Wu, D. He, Q. An, J. Alloys Compd. **699**, 47 (2017)
23. S.U.M. Khan, M. Al-Shahry, W.B. Ingler Jr., Science **297**, 2243 (2002)
24. Y. Fang, M. Sun, Y. Wang, S. Sun, J. He, Mater. Res. Bull. **74**, 265 (2016)
25. K.M. Reddy, B. Baruwati, M. Jayalakshmi, M. MohanRao, S.V. Manorama, J. Solid State Chem. **178**, 3352 (2005)
26. L. Hexing, L. Jingxia, H. Yuning, J. Phys. Chem. B **110**(4), 1559 (2006)
27. K.M. Rajesh, S. Sugunan, J. Appl. Chem. **2**(2), 36 (2012)
28. R. Gomez, T. Lopez, E. Ortiz-Islas, J. Navrrete, E. Sanchez, F. Tzompantzi, X. Bokhimi, J. Mol. Catal. A: Chem. **193**, 217 (2003)
29. F. Galindo, R. Gomez, M. Aguilar, J. Mol. Catal. A: Chem. **281**, 119 (2008)
30. R.K. Manoharan, S. Sankaran, Environ. Sci. Pollut. Res. **25**, 20510 (2018)
31. P. Kubelka, J. Opt. Soc. Am. **38**, 448 (1948)
32. T. Tauc, R. Grigorovici, A. Vancu, Phys. Status Solidi B **15**, 627 (1966)
33. Nie, X., Sohlberg, K.: Materials Research Society Symposium Proceedings on Materials and Technology for Hydrogen Economy, 1–5 December meeting, Boston, MA, pp. 801, 205 (2003)
34. Y. Nakano, T. Morikawa, T. Ohwaki, Y. Taga, Appl. Phys. Lett. **87**, 052111 (2005)
35. D. Dolat, N. Quici, E.K. Nejman, A.W. Morawski, G.L. Puma, Appl. Catal. B: Environ. **115–116**, 81 (2012)
36. Z. Zhang, Z. Huang, X. Cheng, Q. Wang, Y. Chen, P. Dong, X. Zhang, Appl. Surf. Sci. **355**, 45 (2015)
37. C. Randorn, S. Wongnawa, P. Boonsin, Sci Asia **30**, 149 (2004)
38. S. Abbasizadeh, A.R. Keshtkar, M.A. Mousavian, Chem. Eng. J. **220**, 161 (2013)
39. G. Zhang, Y.C. Zhang, M. Nadagouda, C.H. Han, K. O'Shea, S.M. El-Sheikh, A.A. Ismail, D.D. Dionysiou, Appl Catal B: Environ. **144**, 614 (2014)
40. J.G. Yu, G.H. Wang, B. Cheng, M. Zhou, Appl. Catal. B Environ. **69**, 171 (2007)
41. P. Du, A. Bueno-López, M. Verbaas, A.R. Almeida, M. Makkee, J.A. Moulijn, G. Mul, J. Catal. **260**, 75 (2008)
42. Y.H. Ao, J.J. Xu, D.G. Fu, Appl. Surf. Sci. **256**, 239 (2009)
43. Y. Sakatani, H. Ando, K. Okusako, H. Koike, J. Nunoshige, T. Takata, J.N. Kondo, M. Hara, K. Domen, J. Mater. Res. **19**, 2100 (2004)
44. Y.G. Tao, Y.Q. Xu, J. Pan, H. Gu, C.Y. Qin, P. Zhou, Mater. Sci. Eng. **177**, 1664 (2012)
45. S.M. El-Sheikh, G. Zhang, H.M. El-Hosainy, A.A. Ismail, K.E. O'Shea, P. Falaras, A.G. Kontos, D.D. Dionysiou, J. Hazard. Mater. **280**, 723 (2014)
46. X. Guo, D. Mao, G. Lu, S. Wang, G. Wu, J. Mol. Catal. A: Chem. **345**, 60 (2011)
47. V. Etacheri, M. Seery, S. Hinder, G. Michlits, S.A. Pillai, A.C.S. Appl, Mater. Interfaces **5**, 1663 (2013)
48. X.F. Lei, X.X. Xue, H. Yang, C. Chen, X. Li, M.C. Niu, X.Y. Gao, Y.T. Yang, Appl. Surf. Sci. **332**, 172 (2015)
49. B. Neppolian, S.R. Kanel, H.C. Choi, M.V. Shankar, B. Arabindoo, V. Murugesan, Int. J. Photoenergy **5**, 45 (2003)
50. S. Senthilvelan, V.L. Chandraboss, B. Karthikeyan, L. Natanapatham, M. Murugavelu, Mater. Sci. Semicond. Process. **16**, 185 (2013)
51. L. Karimi, S. Zohoori, M.E. Yazdanshenas, J. Saudi Chem. Soc. **18**, 581 (2014)
52. X. Zhang, F. Wu, X. Wu, P. Chen, N. Deng, J. Hazard. Mater. **157**, 300 (2008)
53. S. Liu, J. Yu, M. Jaroniec, J. Am. Chem. Soc. **132**, 11914 (2010)
54. B. Neppolian, H.C. Choi, S. Sakthivel, B. Arabindoo, V. Murugesan, J. Hazard. Mater. **89**, 303 (2002)
55. F.D. Mai, C.S. Lu, C.W. Wu, C.H. Huang, J.Y. Chen, C.C. Chen, Sep. Purif. Technol. **62**, 423 (2008)
56. H. Seshadri, S. Chitra, K. Paramasivan, P.K. Sinha, Desalination **232**, 139 (2008)
57. H.R. Pouretedal, A. Norozi, M.H. Keshavarz, A. Semnani, J. Hazard. Mater. **162**, 674 (2009)
58. J. Liu, L. Han, H. Ma, H. Tian, J. Yang, Q. Zhang, B.J. Seligmann, S. Wang, J. Liu, Sci. Bull. **61**, 1543 (2016)
59. S. Sohrabnezhad, A. Pourahmad, E. Radaee, J. Hazard. Mater. **170**, 184 (2009)
60. F. Li, S. Sun, Y. Jiang, M. Xia, M. Sun, B. Xue, J. Hazard. Mater. **152**, 1037 (2008)
61. H.Y. He, J.F. Huang, L.Y. Cao, J.P. Wu, Desalination **252**, 66 (2010)

62. N. Sobana, M. Swaminathan, Sep. Purif. Technol. **56**, 101 (2007)
63. N. Sobana, K. Selvam, M. Swaminathan, Sep. Purif. Technol. **62**, 648 (2008)
64. S. Ahmed, M.G. Rasul, W.N. Martens, R. Brown, M.A. Hashib, Desalination **261**, 3 (2010)
65. A.V. Petukhov, Chem. Phys. Lett. **277**, 539 (1997)
66. B. Bayarri, J. Gimenez, D. Curco, S. Esplugas, Catal. Today **101**, 227 (2005)
67. E.R. Kusvuran, A. Samil, O.M. Atanur, O. Erbatur, Appl. Catal. B **58**, 211 (2005)